From Two-State to Three-State: The Effect of the P61A Mutation on the Dynamics and Stability of the Factor for Inversion Stimulation Results in an Altered Equilibrium Denaturation Mechanism†

Sarah A. Hobart,‡ Derrick W. Meinhold,‡ Robert Osuna,§ and Wilfredo Colón*,‡

Department of Chemistry, Rensselaer Polytechnic Institute, 110 Eighth Street, Troy, New York 12180, and Department of Biological Sciences, State University of New York at Albany, Albany, New York 12222

Received July 26, 2002; Revised Manuscript Received September 11, 2002

ABSTRACT: Factor for inversion stimulation (FIS) is a 22 kDa homodimeric protein found in enteric bacteria that is involved in the stimulation of certain DNA recombination events and transcription regulation of many genes. FIS has a central helix with a 20° kink, which is only reduced by 4° after a proline 61 to alanine mutation (P61A). This mutation appears to have little effect on FIS function, yet it is striking that proline 61 is highly conserved among *fis* genes. Therefore, we studied the role of proline 61 on the stability and flexibility of FIS. The urea-induced equilibrium denaturation of P61A FIS was monitored by circular dichroism and fluorescence anisotropy. Despite the apparent two-state transition, the concentration dependence of the transition slope (*m* value) shows that a two-state model, as seen for wild-type (WT) FIS, did not adequately describe the denaturation of P61A FIS. Global fitting of the data indicates that the denaturation of P61A FIS occurs via a three-state process involving a dimeric intermediate and has an overall ΔG_{H_2O} for unfolding of 18.6 kcal/mol, 4 kcal/mol higher than that for WT FIS. Limited trypsin proteolysis experiments show that the DNA binding C-terminus of P61A FIS is more labile to cleavage than that of WT FIS, suggesting an increased flexibility of this region in P61A FIS. In contrast, the resulting dimeric core (residues 6−71) of P61A FIS is more resistant to proteolysis, consistent with the presence of a dimeric intermediate not seen in WT FIS. Model transition curves generated using the parameters obtained by global fitting predicted a two-state-like transition at low P61A concentrations that becomes less cooperative with increasing protein concentration, as was experimentally observed. At concentrations of P61A FIS much higher than are experimentally feasible, a biphasic transition is predicted. Thus, this work demonstrates that a single mutation may be sufficient to alter a protein's denaturation mechanism and underscores the importance of analyzing the denaturation mechanism of oligomeric proteins over a wide concentration range. These results suggest that proline 61 in FIS may be conserved in order to optimize the global stability and the dynamics of the functionally important C-terminus.

The role of proline residues on protein structure and function has been a topic of significant interest since the late 1980s. The presence of a proline residue in an α-helix results in a distorted or kinked helix and a loss in protein stability of about 4−7 kcal/mol (*1*−*3*). Presumably, this is due to proline's rigid side chain structure and reduced ability to form hydrogen bonds. Although this property has labeled proline as a helix breaker (*4*), proline is still found in the helices of many proteins (*5*−*8*). Therefore, despite their apparent adverse role on protein stability and structure, the evolutionary conservation of proline residues in α-helices suggests that they may confer unique physical properties that are functionally significant.

Proline residues are commonly found in transmembrane proteins and have been determined to impart a flexibility that is often critical for proper ion-gating function (*9*−*12*). Although proline residues are found less frequently in the helices of globular proteins (*10*), there are globular proteins with well-conserved helical proline residues, such as the heat shock transcription factor (HSF) (*8*), T4 lysozyme (*13*), and thioredoxin (*7*). In HSF and thioredoxin, the proline was found to have little importance for function but exhibited effects on the folding kinetics and conformational stability, respectively (*7*, *8*). Thermal denaturation of HSF showed no effect on stability, but the authors found the proline to be important in preventing aggregation upon overexpression in *Escherichia coli* (*E. coli*) and the accumulation of an aggregate-prone intermediate in the kinetic folding pathway (*8*). In thioredoxin, the proline was found to stabilize the protein by 2.9 kcal/mol through a specific organization of the active site region, although reorganization of the active site upon mutation did not alter its functionality (*7*). These representative cases show that the presence of proline residues in α-helices has diverse effects on protein function, folding, and stability.

† This work was supported by grants from the National Science Foundation (NSF MCB-9984913 to W.C.) and the National Institutes of Health (NIH GM52051 to R.O.). D.W.M. was partially supported by a Howard Hughes Medical Institute undergraduate research program. S.A.H. is a NSF Graduate Fellow.

* Address correspondence to this author. E-mail: colonw@rpi.edu. Fax: (518) 276-4887.

‡ Rensselaer Polytechnic Institute.

§ State University of New York at Albany.

10.1021/bi0265224 CCC: $22.00
Published on Web 10/24/2002

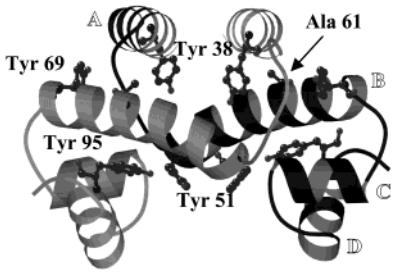

FIGURE 1: Ribbon diagram of the 3D structure of P61A FIS (*6*) from residues 26−98 showing the tyrosine residues and the alanine at position 61. As with the WT protein, the first 25 residues are very mobile, and therefore, the N-terminal structure cannot be resolved by X-ray crystallography in its native sequence. The four α-helices in one subunit are labeled A through D. This figure was prepared using the program MOLSCRIPT (*62*).

Factor for inversion stimulation (FIS)[1] is a 22.4 kDa dimeric DNA binding protein found in *E. coli* and other enteric bacteria (*14*−*16*). It is involved in various cellular processes, including stimulation of site-specific DNA inversion reactions catalyzed by the Hin and Gin family of recombinases (*17*−*19*), stimulation of lambda and HKO22 phage DNA recombination (*20*−*22*), repression of its own transcription and that of various other genes (*23*, *24*), and the stimulation of transcription of ribosomal and tRNA genes and various other structural genes (*24*−*27*). FIS is composed of two identical 98-residue subunits, which form an intertwined dimer of predominantly α-helical structure (Figure 1) (*28*−*30*). The N-terminus of FIS consists of a β-hairpin and helix A and is required for the stimulation of Hin-mediated DNA inversion (*30*−*32*). Helix B, which has a 20° kink, runs through the center of FIS and is responsible for constructing the dimer core, as it makes a number of intermolecular contacts with helices A and B of the other subunit in the dimer. The C-terminal region contains the helix−turn−helix DNA binding motif, involving helices C and D, both of which predominantly interact with helix B of the same subunit.

The kink in helix B is centered on the proline residue at position 61. Interestingly, the kink is only reduced by 4° upon mutation of proline 61 to alanine (P61A) (*6*), and the mutation has little effect on in vivo and in vitro DNA inversion stimulation, as well as no apparent effect on DNA binding (*6*). Although it has been shown that proline residues are often necessary for maintaining the proper helical kink and allowing conformational flexibility in transmembrane proteins (*33*, *34*), the evidence from P61A FIS seems to indicate that this is not the case for FIS (*6*). Nevertheless, proline 61 is strongly conserved in FIS from different bacteria (*35*). To better understand the potential role of proline 61 in FIS that might lead to its high conservation, we decided to study the dynamics, stability, and equilibrium denaturation mechanism of P61A FIS.

[1] Abbreviations: AA, amino acid; CD, circular dichroism; C_m, transition midpoint; far-UV, far-ultraviolet; EDTA, ethylenediaminetetraacetic acid; FIS, factor for inversion stimulation; MALDI, matrix-assisted laser desorption ionization; MS, mass spectrometry; MW, molecular weight; near-UV, near-ultraviolet; P61A, proline to alanine mutation at position 61; PB, potassium phosphate buffer; SDS−PAGE, sodium dodecyl sulfate−polyacrylamide gel electrophoresis; TFA, trifluoroacetic acid; TOF, time of flight; Tris-HCl, tris(hydroxymethyl)-aminomethane hydrochloride; WT, wild type; χ_ν^2, reduced chi squared.

MATERIALS AND METHODS

Protein Expression and Purification. P61A mutation was made by a two-step megaprimer PCR method as previously described (*36*), using *Taq* polymerase (Boerhinger Mannheim) under conditions specified by the manufacturer. In the first reaction, an upstream primer, oRO418 (5′-GAAGTAGAACAG**GCT**CTGTTGGACATG-3′), containing two mutations (bold) specifying a change from the proline codon at position 61 to an alanine codon (underlined), was used together with a second primer, oRO319 (5′-CGGGATCCAAGCATTTAGCTAACC-3′), that anneals to a sequence downstream of the termination codon of *fis* and creates a *Bam*HI recognition sequence. Plasmid pRJ807 (*31*), which carries the wild-type *fis* gene, was used as the DNA template. The product of this PCR was separated by electrophoresis on a 5% polyacrylamide gel and eluted by the crush and soak method (*37*). The purified DNA fragment was used as a megaprimer for a second PCR together with an upstream primer, oRO320 (GGAATTCCATATGTTCGAACAACGCG), that anneals to a sequence at the beginning of *fis* and creates an *Nde*I and an *Eco*RI recognition sequence. The resulting DNA fragment carrying the entire *fis* gene with an alanine codon at position 61 was purified by gel electrophoresis, cleaved with *Nde*I and *Bam*HI, and ligated into the *Nde*I and *Bam*HI sites of the expression vector pET11c (New England BioLabs). The resulting plasmid (pRO425) was transformed into *E. coli* strain RO1106 (*ara* Δ[*lac-pro*] *thi*) *recA56::*Tn*10 srl fis::767 λ*[DE3] F′pro *lacI*^{SQ} Z_{u118}* Tn*5*). The mutation was verified by DNA sequencing using alkali-denatured pRO425 plasmid and Sequenase version 2.0 (U.S. Biochemicals) as specified by the supplier. WT and P61A FIS were overexpressed in *E. coli* and purified as previously described (*38*).

Sample Preparation. WT and P61A FIS concentration (in monomer units) was obtained in 1 M NaCl and 25 mM tris-(hydroxymethyl)aminomethane hydrochloride (Tris-HCl) at pH 7.0, using an extinction coefficient at 278 nm of 6340 M^{-1} cm^{-1} and 6376 M^{-1} cm^{-1}, respectively, determined as previously described (*39*). All experiments were performed at 20 °C in 10 mM potassium phosphate buffer (PB) at pH 7.2 with 0.1 M NaCl, unless otherwise stated. Urea denaturation experiments using 107 μM FIS were carried out at 0.2 M NaCl to prevent the precipitation of FIS that occurs in low salt conditions. We have determined that although 1 M NaCl has a stabilizing effect on FIS, the stability and denaturation mechanism of FIS in the presence of 0.1 or 0.2 M NaCl are virtually the same (data not shown).

Circular Dichroism Studies of P61A FIS. Circular dichroism (CD) spectra were recorded on an OLIS CD instrument (Bogart, GA) equipped with a dual beam optical system. The unfolded structure was observed in 10 mM PB (pH 7.2) and 8 M urea, at 20 °C, and reversibility was verified by returning the sample to native state conditions through a 4-fold dilution.

Equilibrium urea denaturations in the far-ultraviolet (far-UV) were monitored at 222 nm to observe the α-helical content, and 245 nm was used for baseline correction. Far-UV CD denaturations were performed at 0.36 μM (5 cm cell), 1.8 μM (1 cm cell), 8.9 μM (0.2 cm cell), 36 μM (0.1 cm cell), and 107 μM (0.1 cm cell) P61A FIS. Different CD cuvettes were used, depending on the FIS concentration, to obtain sufficient signal to accurately monitor the denaturation.

Denaturation experiments in the near-ultraviolet (near-UV) region were monitored at 277 nm, and 330 nm was used for baseline correction. Near-UV CD denaturations were monitored at 36 and 107 μM P61A FIS, in a 2 and 1 cm cell, respectively. Since the error of the near-UV CD data is larger due to its lower signal, it was not practical to perform denaturation experiments at P61A FIS concentrations below 36 μM. Samples were prepared independently or by a codilution method, in which FIS samples of progressively higher urea concentrations were made by repetitive withdrawal from a FIS sample (originally in 0 M urea) in the cell followed by addition of the same volume of an unfolded FIS solution (8−10 M urea). All CD samples were equilibrated for at least 4 min, which we found to be sufficient time for equilibration. Near-UV CD denaturation experiments at 107 μM were carried out using the codilution method, in which the unfolded FIS stock was in 10.5 M urea, at 40 °C, to keep the urea in solution. P61A is stable at this temperature as its T_m is 76 °C at 2 μM (*6*). The FIS samples were then reequilibrated to 20 °C in the cell prior to collecting the near-UV CD data. Urea concentrations for all experiments were determined from the refractive index measurement using an Abbe refractometer (*40*).

Anisotropy Studies. Steady-state anisotropy was performed on a Hitachi F-4500 fluorescence spectrophotometer (Tokyo, Japan) equipped with Hitachi polarization accessories. Experiments were carried out at 20 °C using a 1 cm pathlength cuvette. Excitation and emission wavelengths were 276 and 305 nm, respectively, with an excitation slit of 5 nm and an emission slit of 10 nm. Equilibrium urea denaturations were performed using the codilution method described for the CD experiments at 8.9, 36, and 107 μM P61A FIS, equilibrating each sample for 4 min prior to recording the signal. For each anisotropy value at least five measurements were recorded and averaged. The integration time was 1 s. Anisotropy was calculated from the formulas:

$$A = (I_{vv} - GI_{vh})/(I_{vv} + 2GI_{vh}) \quad (1)$$

$$G = I_{hv}/I_{hh} \quad (2)$$

where I_{vv}, I_{vh}, I_{hh}, and I_{hv} are the fluorescence intensities when the excitation and emission polarizers, respectively, are set in the vertical (v) or horizontal (h) positions (*41*).

Limited Proteolysis with Trypsin. Limited proteolysis was carried out on P61A and WT FIS at 20 °C using a trypsin to protein ratio of 1:500 (w/w). One reaction sample was made containing 36 μM FIS in reaction buffer [25 mM Tris-HCl, 1 mM ethylenediaminetetraacetic acid (EDTA), pH 7.6] (*42*). Trypsin was diluted into reaction buffer from a concentrated stock (stored frozen in 0.01 M HCl) and added to the FIS sample. Aliquots were removed at times ranging from 0 to 500 min. The cleavage reaction was stopped by mixing 1:1 (v/v) with sodium dodecyl sulfate−polyacrylamide gel electrophoresis (SDS−PAGE) sample buffer, boiling for 2 min, and then freezing the samples (−20 °C) until ready to run on a 16% tricine SDS−PAGE gel to identify the proteolysis fragments.

Proteolyzed FIS samples were analyzed using matrix-assisted laser desorption ionization (MALDI) mass spectrometry (MS). The MS samples were prepared exactly as done for the SDS−PAGE analysis, but the reactions were stopped by adding trifluoroacetic acid (TFA) such that the final concentration of TFA was 0.2% (v/v), then boiled for 2 min, and stored in the freezer until ready to carry out MS. Samples were desalted and concentrated using Millipore brand Zip-Tips (Bedford, MA).

The mass spectra were recorded on a Spec 2E time-of-flight (TOF) instrument (Micromass, Wythenshawe, U.K.). Ionization was achieved using a pulsed N_2 laser at a wavelength of 337 nm. The analyzed solutions were prepared by mixing 1 μL of the sample (~10 pmol/μL), in water with 0.1% TFA, with 1 μL of matrix solution (sinapinic acid or α-cyano-4-hydroxycinnamic acid, 10 mg/mL). Then, 0.5 μL of this solution was applied to the target. Mass spectra were recorded in linear mode, with accuracy on the mass measurements of around 0.1%.

Data Modeling. For comparison of data collected with different spectral methods (Figure 4), the data was normalized to F_u, the apparent fraction of unfolded protein

$$F_u = (Y_o - Y_n)/(Y_u - Y_n) \quad (3)$$

where Y_o is the signal at a given urea concentration and Y_n and Y_u are the observed values for the native and unfolded protein, respectively. The terms Y_n and Y_u are defined as linear equations specifying the urea dependence on the baseline slopes. For comparison of data collected by the same technique but at different protein concentrations (Figures 2 and 3), the data were internally normalized, using the first and last data points as Y_n and Y_u, respectively. By using this method of normalization, instead of calculating F_u (eq 3), we were able to preserve the original baseline slopes.

The data from the urea denaturation experiments were fit to a two-state dimer model, with native dimer (N_2) in equilibrium with unfolded monomers (2U):

$$N_2 \leftrightarrow 2U \quad (4)$$

The equilibrium constant for concerted unfolding and dissociation, K_u, is defined as $K_u = [U]^2/[N_2]$. The total protein concentration, P_t, in terms of monomer is $P_t = 2N_2 + U$, and the fraction of native dimers (F_n) = $1 - F_u$, where $F_u = [U]/P_t$. Combining these equations and solving for F_u in terms of the equilibrium constant K_u and P_t, one obtains

$$F_u = \frac{\sqrt{K_u^2 + 8K_uP_t} - K_u}{4P_t} \quad (5)$$

Rearranging eq 3 yields the equation used for fitting the denaturation transitions:

$$Y_o = Y_n(1 - F_u) + Y_u(F_u) \quad (6)$$

The thermodynamic parameters listed in Table 1 were obtained by fitting the denaturation curves to eq 6, with F_u as defined in eq 5. K_u was defined according to the linear free energy model, which states that the changes in free energy (ΔG_u) that accompany protein unfolding are linearly dependent on the concentration of urea denaturant (*43*, *44*):

$$\Delta G_u = -RT \ln(K_u) = \Delta G_{H_2O} + m[\text{denaturant}] \quad (7)$$

The baseline slopes and intercepts were used as fitting variables as shown in eq 6, in addition to m and ΔG_{H_2O}. Fits

Table 1: Thermodynamic Analysis of Equilibrium Denaturation Data Based on a Two-State Model[a]

method	$[P_t]$ (μM)	C_m (M urea)	m value [kcal/(mol M)]	ΔG_{H_2O} (kcal/mol)
far-UV CD	0.36[b]	4.60 ± 0.06	2.15 ± 0.14	18.6 ± 1.2
	1.8	5.16 ± 0.03	1.89 ± 0.12	17.6 ± 1.1
	9.0	5.65 ± 0.11	1.52 ± 0.24	15.5 ± 2.5
	36	5.95 ± 0.06	1.46 ± 0.11	14.8 ± 1.1
	107	6.14 ± 0.10	1.40 ± 0.11	14.1 ± 1.1
near-UV CD	36	5.84 ± 0.15	1.79 ± 0.45	16.5 ± 4.2
	107	5.94 ± 0.26	1.13 ± 0.26	12.1 ± 2.8
anisotropy	9	5.52 ± 0.10	1.71 ± 0.28	14.1 ± 2.3
	36	5.95 ± 0.13	1.50 ± 0.16	15.0 ± 1.6
	107	6.24 ± 0.09	1.29 ± 0.14	13.5 ± 1.5

[a] The ΔG_{H_2O} is defined by $mC_m - [RT \ln[P_t]]$. Urea denaturation profiles were analyzed according to the linear free energy model. Errors are based on averaged data from at least three individual experiments. [b] The 0.36 and 1.8 μM data were collected using a 5 and 2 cm cuvette, respectively, to amplify the signal to obtain reproducible and reliable data.

of individual data sets to the two-state model were performed with KaleidaGraph v3.5 (Synergy Software).

Global analysis of the P61A FIS equilibrium urea denaturation data was fit to both possible three-state denaturation models, in which the native dimer (N_2) is in equilibrium with either a monomeric (2I) or dimeric intermediate (I_2) and the unfolded monomers (2U):

$$N_2 \leftrightarrow I_2 \leftrightarrow 2U \tag{8}$$

$$N_2 \leftrightarrow 2I \leftrightarrow 2U \tag{9}$$

For a three-state model involving a dimeric intermediate (eq 8), the equilibrium constants for the first (K_1) and second (K_2) transitions are defined as $K_1 = [I_2]/[N_2]$ and $K_2 = [U]^2/[I_2]$, respectively. The total protein concentration, P_t, in terms of the monomer, is $P_t = 2N_2 + 2I_2 + U$, and the sum fraction of native dimers (F_n), intermediate dimers (F_i), and unfolded monomers (F_u) at equilibrium is equal to 1. Through a combination of these relationships, one obtains the equations:

$$K_1 = F_i/F_n \tag{10}$$

$$K_2 = 2P_t F_u^{\,2}/F_i \tag{11}$$

F_u can be solved for in terms of P_t, K_1, and K_2 by solving for F_i and F_n solely in terms of F_u, K_1, K_2, and P_t:

$$F_u = \frac{-K_1K_2 + \sqrt{(K_1K_2)^2 + 8(1 + K_1)(K_1K_2)P_t}}{4P_t(1 + K_1)} \tag{12}$$

The fitting equation is an expression similar to eq 6 but with an extra term defining the intermediate:

$$Y_o = Y_n\left(\frac{2P_tF_u^{\,2}}{K_1K_2}\right) + Y_i\left(\frac{2P_tF_u^{\,2}}{K_2}\right) + Y_u(F_u) \tag{13}$$

Combining eqs 7, 12, and 13, it is possible to extract the m value (slope of the transition) and the ΔG_{H_2O} for each step in the reaction.

For a three-state model involving a monomeric intermediate (eq 9), the equilibrium constants for the first (K_1) and second (K_2) transitions are defined as $K_1 = [I]^2/[N_2]$ and $K_2 = [U]/[I]$. The total protein concentration, P_t, in terms of the monomer, is $P_t = 2N_2 + I + U$, and again $F_n + F_i + F_u = 1$. Through a combination of these relationships, one obtains the equations:

$$K_1 = 2P_tF_i^{\,2}/F_n \tag{14}$$

$$K_2 = F_u/F_i \tag{15}$$

F_i can be solved for in terms of P_t, K_1, and K_2 by solving for F_u and F_n solely in terms of F_i, K_1, K_2, and P_t:

$$F_i = \frac{-K_1(1 + K_2) + \sqrt{K_1^{\,2}(1 + K_2)^2 + 8P_tK_1}}{4P_t} \tag{16}$$

The fitting equation is an expression similar to eq 13 but with the terms defined as is appropriate for this model:

$$Y_o = Y_n\left(\frac{2P_tF_i^{\,2}}{K_1}\right) + Y_i(F_i) + Y_n(K_2F_i) \tag{17}$$

Combining eqs 7, 16, and 17, it is possible to extract the m value and the ΔG_{H_2O} for each step in the reaction. Y_i is assumed to not vary with denaturant concentration in both three-state models.

Global analysis of the data was done by simultaneously fitting all the data at different FIS concentrations from the different methods to the three models described above. This analysis was carried out using the program SAVUKA version 5.1, a nonlinear least-squares fitting program (*45*, *46*). The goodness of fit was determined by analyzing the reduced χ^2 values (χ_ν^2):

$$\chi_\nu^{\,2} = \frac{\sum([y_i - y(x_i)]^2/\sigma^2)}{\nu} \tag{18}$$

where y_i is the data, $y(x_i)$ is the fit to the data, σ^2 is the variance of the data, and ν is the number of degrees of freedom in the fit (*47*). The F-test was performed by taking the ratio of the χ_ν^2 from the fit of each model to the data (*48*). We modeled the three-state denaturation mechanism of FIS with Microsoft Excel version 8.0, using the equations described above and the ΔG_{H_2O}, m values, and Y_i obtained from global analysis.

RESULTS

Equilibrium Denaturation Experiments. The denaturation of P61A FIS was monitored using various techniques to observe the loss of secondary, tertiary, and quaternary structure. The reversible (see inset in Figure 2A) loss of helical structure with increasing urea concentrations was monitored by far-UV CD (222 nm) over a wide range of P61A FIS concentrations (Figure 2A) to determine if the loss of secondary structure is dependent on the dissociation of the dimer. The unfolding of P61A FIS, as determined by the loss of helical signal, appears to be a concerted, concentration-dependent event, as previously shown for WT FIS (*38*). A dramatic increase in the transition midpoint (C_m) of P61A over that of WT FIS suggests a significant enhancement in secondary structure stability (Figure 2A). However, as the protein concentration is increased, both the

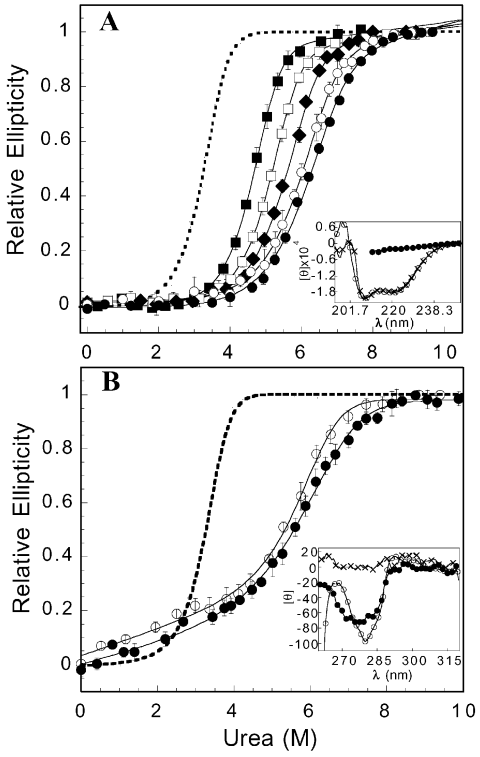

FIGURE 2: Urea-induced denaturation of P61A FIS monitored by (A) far-UV CD at 222 nm and (B) near-UV CD at 277 nm. The data were internally normalized as described in Materials and Methods. FIS concentrations are 0.36 μM (■), 1.8 μM (□), 8.9 μM (◆), 36 μM (○), and 107 μM (●). The dashed line indicates the urea denaturation transition for a 36 μM sample of WT FIS for comparison (*38*). Error bars represent the average of at least three individual data sets. The solid lines on the denaturation curves indicate a two-state fit of the data as described in Materials and Methods. The insets in (A) and (B) show the full wavelength scans in the far- and near-UV regions, respectively. The molar ellipticity, [θ], has units of deg·cm^2·dmol^{-1}. The symbols in inset A represent the full spectrum of native (○), unfolded in 6 M urea (●), and refolded (×) P61A FIS. The symbols in inset B represent the full spectrum of native P61A (●), WT (○), and unfolded (×) P61A FIS.

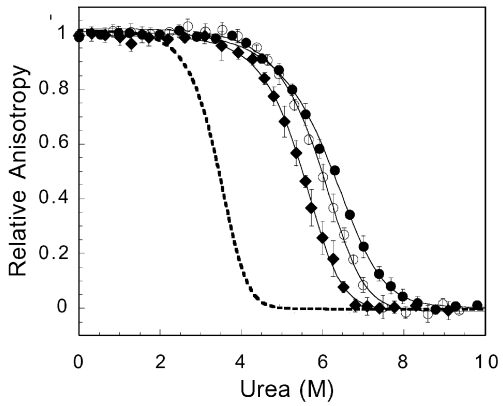

FIGURE 3: Urea-induced denaturation of P61A FIS monitored by steady-state anisotropy at 8.9 μM (◆), 36 μM (○), and 107 μM (●). The data were internally normalized as described in Materials and Methods. The solid lines indicate a two-state fit as described in Materials and Methods. Error bars represent the average of at least three individual data sets. The dashed line represents the anisotropy urea denaturation transition of 36 μM WT FIS (*38*).

slope (*m* value) of the transitions and the concentration dependent change in the C_m values decrease. These observations are not expected to occur in a two-state denaturation mechanism and, thereby, suggest the presence of an intermediate. Therefore, to further probe for the presence of an intermediate, we also monitored the denaturation of P61A FIS using near-UV CD and tyrosine fluorescence anisotropy.

The near-UV CD signal provides a convenient way to monitor changes in protein tertiary structure, as the specific environment of aromatic residues in the native state is unique for every protein (*49*). The near-UV CD spectrum of FIS arises from the different contributions of the protein's four tyrosine residues that are positioned throughout the protein (Figure 1). The near-UV CD spectra of WT and P61A FIS (see inset in Figure 2B) are noticeably different, indicating a different arrangement or mobility of one or more tyrosine residues. The equilibrium unfolding of P61A FIS monitored by near-UV CD (277 nm) at 36 and 107 μM shows a loss of signal throughout the pretransition baseline upon addition of urea, prior to the main unfolding transition (Figure 2B). Since near-UV CD can monitor the loss of chirality in the environment of tryptophan and tyrosine residues resulting from increased rotational freedom of these residues (*50*), the sloped baselines in Figure 2B suggest that a relaxation of the P61A FIS structure is occurring at low urea concentrations prior to the main unfolding event. This suggests that the P61A FIS mutant possesses an increased conformational flexibility that is absent in WT FIS (dash line in Figure 2B) (*38*), which exhibit flat near-UV CD pretransition baselines.

Intrinsic fluorescence measurements were not feasible for monitoring the denaturation of P61A FIS because of the very small signal change between the native and unfolded states. Therefore, the equilibrium unfolding mechanism of P61A FIS was furthered explored by steady-state anisotropy (Figure 3). Upon subunit dissociation, the anisotropy signal is expected to decrease, mostly due to a decrease in the correlation time of the rotating fluorophores. Changes in anisotropy usually cannot be directly correlated with the fraction of dissociated or unfolded species due to changes in fluorophore quantum yield, the lifetime of the excited state, or fluorophore side chain mobility upon unfolding (*41*). In FIS, these effects can be considered minimal due to the similar fluorescence intensities of the native and unfolded states and the partial exposure of all four FIS tyrosines in the native state (Figure 1). Therefore, it is likely that the majority of the decrease in FIS anisotropy signal, upon addition of urea, arises from changes in quaternary structure. As expected, the anisotropy-monitored denaturation of P61A FIS occurs in a concerted and concentration-dependent manner.

A representative overlay (36 μM data) of the P61A FIS equilibrium denaturation data from different methods is plotted in Figure 4 along with an overlay of the far-UV CD transition of WT FIS at 36 μM (*6*). The small shift to the left of the P61A FIS near-UV CD transition may suggest a deviation from two-state denaturation, although there are larger errors in this data due to the low signal. Consistent with this suggestion, Table 1 shows that, for the far-UV CD and anisotropy data, the *m* values become consistently smaller upon increasing the protein concentration, indicating a deviation from two-state behavior. A *t*-test was performed (*47*, *51*) to determine the probability that the differences in the *m* values are real and not caused by chance. Although

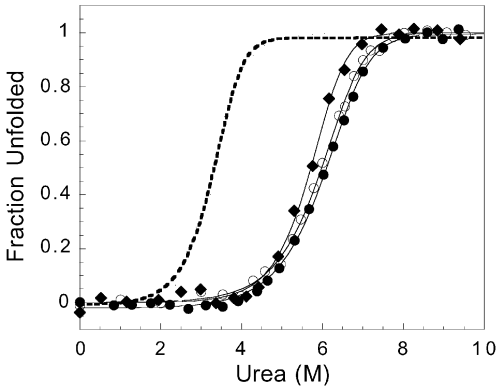

FIGURE 4: An overlay of the urea denaturation curves of P61A FIS at 36 μM determined by far-UV CD (●), near-UV CD (◆), and anisotropy (○). The data are displayed as fraction unfolded determined as described in eq 3. The dashed line represents the far-UV CD urea denaturation transition of 36 μM WT FIS (*38*). The solid lines indicate a two-state fit as described in Materials and Methods.

for any two consecutive concentrations (e.g., 1.89 and 1.52 μM in far-UV CD) the *t*-test gives a high probability that the corresponding *m* values are not statistically different, the differences in *m* values between the highest two and lowest two concentrations used in far-UV CD experiments have a probability of <0.05 to have been caused by chance. Similar *t*-test results were obtained for the highest and lowest *m* values determined by anisotropy.

It has been shown for many monomeric proteins that a decrease in the *m* value of a mutant protein compared to the WT is due to the population of an intermediate (*52*−*55*). A similar concept can be applied to dimeric systems by investigating the concentration dependence of the denaturation transitions. When protein denaturation transitions are biphasic, the individual transition curves may be fit reliably to a specific model. However, since in P61A FIS the presence of an intermediate is less obvious, global fitting provides the most reliable method for analyzing the data to identify the appropriate model and extract the corresponding thermodynamic parameters.

The data in Figures 2 and 3 were globally fit to a two-state denaturation mechanism, as well as both possible three-state equilibrium denaturation models involving either a dimeric or a monomeric intermediate. Figure 5 is shown to illustrate how well these various models fit the P61A FIS data. Only the far-UV CD data are plotted to emphasize the quality of the fit at five different protein concentrations. All of the data plotted in Figure 5 had both of the far-UV CD baselines constrained to zero slope during global analysis in order prevent the algorithm from generating baseline artifacts in an attempt to force a good fit onto the data. These plots show that a three-state mechanism involving a dimeric intermediate is most consistent with the data. By comparison of the ratio of the reduced χ^2 obtained from fitting the data to different models (Figure 5), an *F*-test (*47*, *48*) predicts that the three-state model involving a dimeric intermediate is a statistically superior fit with greater than 99% probability. Table 2 shows the thermodynamic parameters from this fit, which results in a ΔG_{H_2O} of 6.1 and 12.5 kcal/mol for the $N_2 \leftrightarrow I_2$ and $I_2 \leftrightarrow 2U$ transitions, respectively. The global fitting indicates that the dimeric intermediate retains 70% of the native signal (see footnote to Table 2).

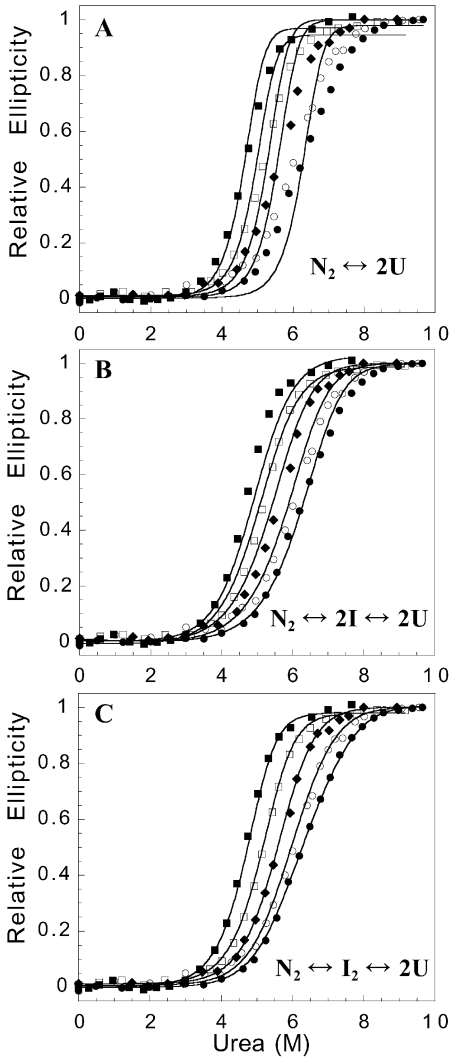

FIGURE 5: The global fitting of the P61A FIS data to the three equilibrium denaturation models shown above. The symbols represent the far-UV CD data at 0.36 μM (■), 1.8 μM (□), 8.9 μM (◆), 36 μM (○), and 107 μM (●) P61A FIS. The lines represent the fit of the various models to the far-UV CD data, with the far-UV CD native and unfolded baselines constrained to zero slope to prevent fitting artifacts in the baseline regions. Only the far-UV CD data are shown for ease of visualizing the fits across a wide concentration range. Using the reduced χ^2 for the $N_2 \leftrightarrow 2U$ (12.03), $N_2 \leftrightarrow 2I \leftrightarrow 2U$ (1.98), and $N_2 \leftrightarrow I_2 \leftrightarrow 2U$ (0.68) models, an *F*-test predicts that the $N_2 \leftrightarrow I_2 \leftrightarrow 2U$ is statistically the best fit to the data.

Limited Proteolysis of P61A FIS by Trypsin. In an attempt to compare the flexibility of P61A and WT FIS and to gain some structural insight on the dimeric intermediate of P61A FIS, we carried out limited proteolysis experiments. Figure 6 shows the differences in the trypsin proteolytic cleavage patterns between WT and P61A FIS as analyzed by SDS−PAGE. The initial cleavage of FIS generates two core fragments of about 7−8 kDa (Figure 6), which arise faster in P61A than in WT FIS. However, the subsequent cleavage of the core fragments is much slower for P61A FIS. This result suggests that P61A FIS is initially more labile to proteolysis due to an area of increased flexibility compared to WT FIS. However, the resulting core fragment of P61A FIS is more stable and rigid compared to the WT protein, making it more resistant to proteolysis.

Table 2: Equilibrium Denaturation Global Analysis[a]

protein	$\Delta G_{N_2 \leftrightarrow I_2}$ (kcal/mol)	$m_{N_2 \leftrightarrow I_2}$ [kcal/(mol M)]	$\Delta G_{I_2 \leftrightarrow 2U}$ (kcal/mol)	$m_{I_2 \leftrightarrow 2U}$ [kcal/(mol M)]	$\Delta G_{N_2 \leftrightarrow 2U}$ (kcal/mol)	$m_{N_2 \leftrightarrow 2U}$ [kcal/(mol M)]
P61A[b]	6.1 ± 0.3	1.03 ± 0.05	12.5 ± 0.4	1.10 ± 0.06	18.6 ± 0.5	2.13 ± 0.08
WT					14.2 ± 0.2	2.40 ± 0.06

[a] Global analysis was performed with SAVUKA version 5.1, a nonlinear least-squares fitting program (*45*, *46*). [b] The relative optical signal (Y_i) of the intermediate state was calculated to be 0.27, where the signal for the native (Y_n) and unfolded (Y_u) states is 0 and 1, respectively.

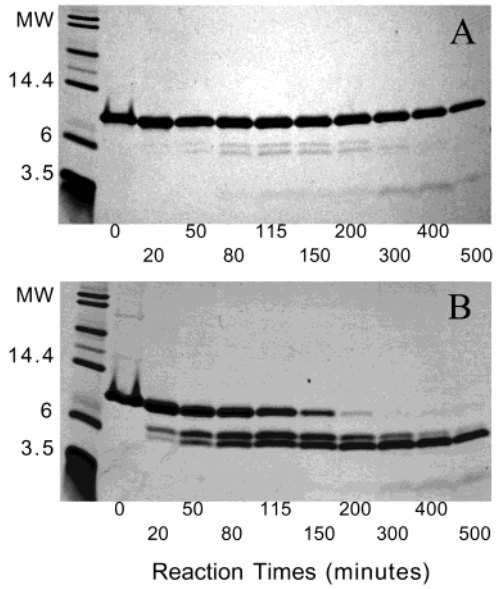

FIGURE 6: Limited trypsin cleavage of (A) WT and (B) P61A FIS at 20 °C, with a 1:500 (w/w) trypsin:protein ratio, was monitored by SDS−PAGE. Aliquots from the reacting sample were removed and the reactions stopped at the times indicated on the gels.

Mass spectrometry was carried out to identify the trypsin cleavage fragments seen by SDS−PAGE (Figure 6). From the mass of the main peaks, W1 and P1 (Figure 7, Table 3), it is clear that the first cleavage, occurring within 50 min on both WT and P61A FIS, removes the first five residues (Table 3). The remaining native-like fragment is indistinguishable from native FIS on SDS−PAGE (Figure 6). The main cleavage of this native-like FIS fragment occurs on the C-terminal region of FIS resulting in two core fragments, residues 6−71 and 6−76 (Table 3). The smallest fragments observed in the gels (Figure 6), with masses under 3 kDa, correspond to the fragments comprising residues 6−28 and 6−32.

DISCUSSION

P61A FIS Denaturation Mechanism. When the denaturation of P61A at a single concentration is monitored by different methods, the transition appears to occur in a two-state fashion due to the coincidence of the data (Figure 4). However, it is expected that if the denaturation mechanism is two-state, then the *m* value and ΔG_{H_2O} of each transition should be the same at all concentrations examined (*56*, *57*). This is what we observe for WT FIS (*38*). In contrast, when the P61A FIS data are analyzed according to a two-state model, a decrease in *m* value upon increasing the protein concentration (from 0.34 to 107 μM for far-UV CD) was observed (Table 1). Also, upon close examination of the far-UV CD denaturation curves (Figures 2A), which were carried out over a broad concentration range, it appears that the transitions begin to lose their concentration dependence at the highest protein concentrations studied. Since sample preparation, data collection, and data analysis were identical for WT (*6*) and P61A FIS, it is unlikely that the changing *m* value observed for P61A FIS is due to an artifact or experimental error. Thus, a two-state model does not adequately describe the equilibrium denaturation of P61A FIS.

As was suggested earlier by fitting the individual denaturation curves to a two-state denaturation mechanism (Table 1), the global fitting results (Figure 5A) show that this model is not consistent with the P61A FIS data. Since a two-state model assumes that *m* values will not change with protein concentration, it is not surprising that such a model fits the P61A FIS data poorly (Figure 5A), especially at the highest protein concentrations where the transition is significantly less cooperative (lower *m* value).

The global fitting analysis also demonstrates that a three-state denaturation mechanism involving a monomeric intermediate is inconsistent with the P61A FIS data (Figure 5B). There is also an argument based on fundamental equilibrium concepts that would rule out a monomeric intermediate. If the P61A FIS intermediate were monomeric, it would be expected that as the protein concentration is increased, the first transition ($N_2 \leftrightarrow 2I$) would be stabilized with respect to the second transition ($2I \leftrightarrow 2U$), whereas at lower protein concentration, the opposite would occur. Therefore, the concentration dependence and two-state likeness of the transitions would increase at higher protein concentrations and decrease at lower protein concentrations. The P61A FIS data exhibit the opposite trend. Thus, the monomeric intermediate model contradicts the raw P61A FIS denaturation data, as can be seen in Figure 5B where this model predicts less concentration-dependent data at low protein concentrations, where the experimental transition curves are actually becoming more concentration dependent and more cooperative.

Global analysis indicates that a three-state model involving a dimeric intermediate is the most consistent with the P61A FIS denaturation data, as is demonstrated in Figure 5C by the excellent fit through the data points. This was shown to be a statistically relevant improvement of the fit, with greater than 99% probability, according to the *F*-test. The analysis reveals that the $N_2 \leftrightarrow I_2$ and $I_2 \leftrightarrow 2U$ transitions have a ΔG_{H_2O} of 6.1 and 12.5 kcal/mol, respectively; both transitions have *m* values of about 1 kcal/(mol M) (Table 2). The absence of a biphasic transition, even at the highest concentrations that we are able to study, indicates that the two conformational events are coupled. The global fit computes that the dimeric intermediate has lost around 30% of the native signal ($Y_n = 0$, $Y_i = 0.30$, $Y_u = 1$). Even though one would expect that different spectroscopic probes would yield a different signal for the dimeric intermediate, the signal did not change when

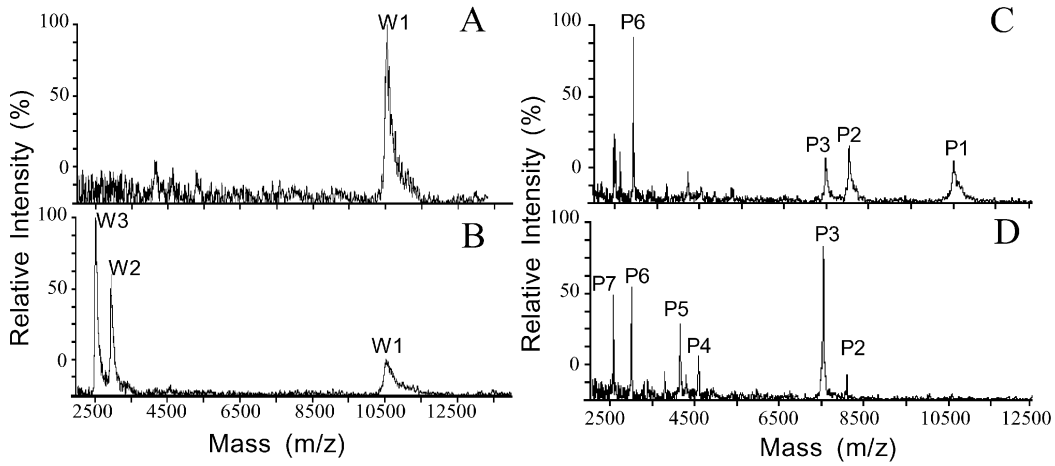

FIGURE 7: Limited trypsin cleavage of WT and P61A FIS at 20 °C, with a trypsin:protein ratio of 1:500 (w/w), was monitored by MALDI-MS. The WT FIS data are presented in (A) and (B) and represent cleavage at 50 and 500 min, respectively. P61A FIS data are presented in (C) and (D) and represent cleavage at 50 and 400 min, respectively. The peaks in MALDI-MS spectra are labeled numerically, in which a W or P in the fragment label indicates that the fragment is of WT or P61A FIS, respectively.

Table 3: MALDI-TOF MS Analysis of Limited Trypsin Digest

label	fragments (AA[a] positions)	average molecular mass	
		calcd	obsd
W1[b]	6−98	10549	10544
W2	6−32	2959	2951
W3	6−28	2530	2527
P1[c]	6−98	10523	10518
P2	6−76	8046	8044
P3	6−71	7490	7487
P4	33−71	4549	4547
P5	37−71	4109	4105
P6	6−32	2959	2955
P7	6−28	2530	2525

[a] AA stands for amino acid. [b] A W in the fragment label indicates the fragment is from WT FIS. [c] A P in the fragment label indicates the fragment is from P61A FIS.

the far-UV CD, near-UV CD, and anisotropy data were analyzed separately by global fitting (data not shown). In the case of FIS, these results can be explained by looking at the crystal structure of P61A FIS (Figure 1). The predicted 30% signal loss in the far-UV CD signal upon formation of the dimeric intermediate correlates well with the unfolding of the C and D helices, which make up about 33% (18 out of 54 residues) of the helical content of FIS. This C-terminal subdomain is the most likely region to become unstructured upon formation of the dimeric intermediate because it is largely involved in intramolecular interactions (Figure 1) and has been shown by proteolysis to be the most flexible region of the protein (Figure 6, Table 3). Mutational studies (unpublished results) indicate that 25−35% of the fluorescence of FIS arises from tyrosine 95, which is the only tyrosine located at the C-terminus (Figure 1). Therefore, a 30% change in anisotropy signal upon the formation of I_2 is also consistent with the data. Furthermore, the 30% change in the near-UV CD signal associated with the pretransition baseline (Figure 2B) is also consistent with the global fitting data and is apparently reporting on the conformational flexibility of the C-terminus. This is also supported by the proteolysis experiments (Figure 6, Table 3) and our observations from mutational studies involving the four tyrosine residues (unpublished results) that most of the FIS near-UV CD signal arises from tyrosines 51 and 95. Thus, it appears that the conformational change associated with the formation of the P61A FIS dimeric intermediate involves the C-terminal region, which accounts for about 30% of the various spectroscopic signals. The unfolding of the C and D helices of P61A FIS to form a dimeric intermediate is consistent with the similar *m* values (Table 2) of the $N_2 \leftrightarrow I_2$ and $I_2 \leftrightarrow 2U$ transitions, since the unfolding of this region would expose part of helix B against which it packs (Figure 1) in the native state.

Using the ΔG's, *m* values, and the optical signal of the dimeric intermediate obtained by global fitting, combined with the three-state denaturation equations described in Materials and Methods, we modeled the fraction of populated P61A FIS species at different concentrations (Figure 8). At lower protein concentrations (0.36 μM), the denaturation is nearly two-state because of the similar C_m values of the $N_2 \leftrightarrow I_2$ and $I_2 \leftrightarrow 2U$ transitions, which leads to low population of the intermediate (Figure 8A). For this reason, when the lower concentration data are analyzed using a two-state model, the *m* values and ΔG_{H_2O}'s match closely to the global parameters determined using the three-state model with a dimeric intermediate (Tables 1 and 2). However, as the concentration of P61A FIS is increased, the C_m of the $I_2 \leftrightarrow 2U$ transition moves further to the right, thereby partially separating the $N_2 \leftrightarrow I_2$ and $I_2 \leftrightarrow 2U$ transitions (Figure 8B). Although the transitions are less coupled at the highest concentrations studied, there still is a significant overlap. It is for this reason that we observe a broadening of the transition and, consequently, a lower *m* value, as opposed to a biphasic transition. Modeling predicts that, at P61A FIS concentrations higher than experimentally feasible, the denaturation transition would become biphasic (Figure 8C).

Increased Flexibility of the P61A FIS C-Terminal Region. The baseline slopes present in the near-UV CD denaturation data suggest that the P61A mutation has increased the flexibility of the C-terminal subdomain of FIS. Although the pretransition slope of the near-UV CD data could be caused by very subtle structural effects that are propagated through the protein, the loss of near-UV CD signal in the absence of changes in the far-UV CD signal is often interpreted as arising from changes in environmental asymmetry near the aromatic residue due to conformational fluctuation (*50*).

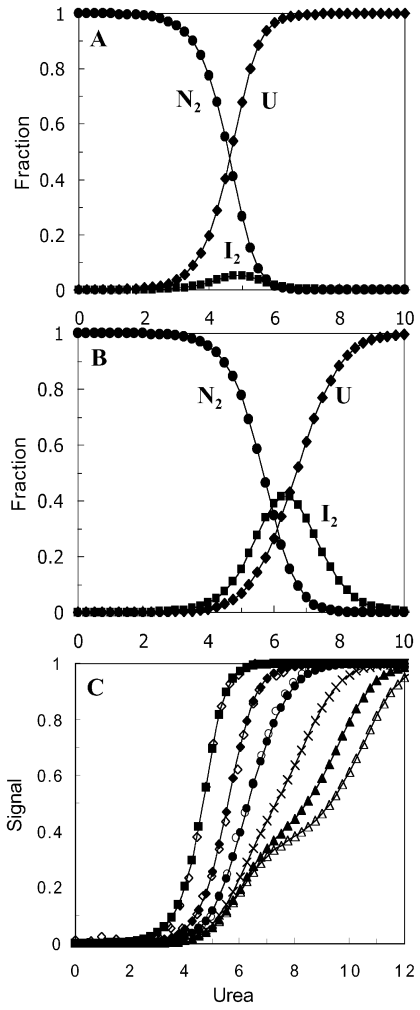

FIGURE 8: Fractions of native (N_2, ●), intermediate (I_2, ■), and unfolded (U, ◆) P61A FIS as a function of urea concentration at (A) 0.36 μM and (B) 107 μM. Panel C shows the theoretical signal that would be obtained from the three-state model $N_2 \leftrightarrow I_2 \leftrightarrow 2U$ at 0.36 μM (■), 8.9 μM (◆), 107 μM (●), 1.78 mM (×), 180 mM (▲), and 890 mM (△). The open symbols at 0.36, 8.9, and 107 μM represents the far-UV CD data. The modeled fractions and signals were calculated using the data in Table 2 and the three-state equations described in Materials and Methods.

Perhaps the best example of this is the molten globule state of proteins, which is characterized by being highly flexible (no near-UV CD signal) while retaining native-like secondary structure (i.e., no change in far-UV CD signal) (*50*, *58*). Since the pretransition baseline of WT FIS is not sensitive to urea, it is probable that this area of presumably increased flexibility in P61A FIS is associated with the proposed dimeric intermediate.

Since limited proteolysis is a convenient method to monitor the changes in protein flexibility upon mutation (*59*), we used trypsin proteolysis combined with SDS−PAGE and MALDI-TOF MS analysis to probe the flexibility of the C-terminal subdomain of P61A FIS. The results demonstrate that WT FIS has a more rigid structure in its native state than P61A (Figure 6). The native-like WT FIS band is persistent after 500 min of treatment, whereas in P61A FIS, the band is almost completely proteolyzed by 200 min. However, the resulting WT FIS core fragments, residues 6−76 and 6−71, are very unstable compared to the corresponding P61A FIS core fragments. These core fragments, seen in both WT and P61A FIS, are the result of the cleavage of the C-terminal DNA binding region (Figures 6 and 7, Table 3). Therefore, we propose that the C-terminal region of P61A FIS has more dynamic fluctuations than in WT FIS, thereby resulting in greater accessibility to trypsin. The increased dynamics of P61A FIS is consistent with the sloped native state baseline seen in the near-UV CD denaturation curves (Figure 2) and the difference in the near-UV CD spectra between WT and P61A FIS (see inset in Figure 2). This simultaneous increase in mobility of the C-terminal region and the increased stability of the dimer core in P61A FIS is also consistent with the observed three-state equilibrium denaturation. Although it is not clear why the C-terminus of P61A may be more flexible than WT, it appears that the small change in kink angle (*6*) of helix B has disrupted the intramolecular salt bridge between K94 (D helix) and E52 (beginning of helix B), as suggested by the increased distance between these two residues in P61A FIS. The importance of this salt bridge in the stability of FIS has been suggested by a K94A FIS mutant, which is significantly less stable than WT and exhibits increased proteolytic susceptibility at its C-terminus, similar to that of P61A FIS (unpublished results).

Role of Proline 61 in FIS Stability. The overall ΔG_{H_2O} for unfolding of P61A FIS is 18.6 kcal/mol, which is about 4 kcal/mol higher than that of WT FIS (Table 2). The observed destabilizing effect of proline 61 in WT FIS is consistent with previous studies demonstrating protein destabilization due to the presence of proline residues in α-helices (*1*−*3*). The increased stability of P61A FIS most likely results from a stabilization of the B helix, which, in turn, stabilizes the whole protein through intra- and intermolecular interactions with other regions of FIS. However, despite its greater stability, the equilibrium denaturation mechanism of P61A FIS is more complex than that of WT. Our data suggest that the C-terminus of P61A FIS was stabilized by the mutation but not to the same extent as the B helix dimer core. If the C-terminus of P61A were not stabilized by the mutation, it would be expected to unfold at around 3.3 M urea (at 36 μM), as seen for WT FIS. In contrast, the equilibrium unfolding of P61A FIS does not begin to occur until 4 M urea, a concentration of urea where WT FIS is nearly 100% unfolded. Despite the increase in overall stability, the slope in the near-UV CD pretransition baseline and the rapid proteolytic cleavage of the C-terminal region suggest that the C-terminus of P61A FIS is also more dynamic than that of WT FIS. Therefore, the differential stabilization and flexibility of the various P61A FIS subdomains appear to give rise to its three-state denaturation mechanism.

Is Proline 61 Important for FIS Function? A comparison of FIS amino acid sequences from 11 bacterial species revealed that proline 61 is fully conserved among these species (*35*). This conservation is most striking in *Pseudomonas aeruginosa* and *Neisseria meningitidis* where the overall FIS amino acid sequences diverged from that in *E. coli* by about 55% and 67%, respectively. Such a strong conservation of proline 61 is quite remarkable given the destabilizing effect generally attributed to the presence of proline in α-helices and suggests that it may be subject to some selective pressure.

Previous work showed that serine or leucine substitutions at this position severely reduced the ability of FIS to stimulate DNA inversion while having modest effects on DNA

binding, suggesting that a polar or bulky nonpolar side chain at this position can significantly alter the structure or stability of the N-terminal region responsible for stimulating DNA inversion (*31*, *32*). However, P61A showed only a modest decrease in the ability to stimulate Hin-mediated DNA inversion in vivo when expressed from the P_{tac} promoter on a multicopy plasmid, and purified P61A FIS showed a small decrease regarding this same function in vitro (*6*). This suggested that the critical structural elements required for this activity in WT FIS are not substantially altered in P61A FIS. Nevertheless, the greater susceptibility of P61A FIS to proteolysis in vitro compared to the WT protein (Figure 6) could be indicative of a greater turnover rate in vivo. If so, this could significantly reduce the available intracellular pool of this protein, particularly if expressed from its own promoter as a single chromosomal copy.

CONCLUSION

The B helix is the structural pillar that holds the FIS intertwined dimer together, as it is involved in extensive intra- and intermolecular interactions (Figure 1). Therefore, the P61A mutation in the middle of helix B significantly stabilizes (>4 kcal/mol) the global structure of FIS, as clearly indicated by the near doubling of the C_m values (5.95 M at 36 μM, Table 1) over that of WT FIS (3.3 M at 36 μM) (*6*). However, two unexpected results of the P61A mutations were the increase in flexibility of the C-terminal DNA binding subdomain and the alteration of the denaturation pathway of FIS from two-state to three-state. The limited proteolysis/MS experiments suggest a more fluctuating P61A FIS C-terminus rather than an altered structure since the 3D structure and function of P61A FIS (*6*) are very similar to those of WT FIS. This increased flexibility is probably caused by a weakening of the important salt bridge between K94 and E52 that occurs due to the small decrease in the kink angle (*6*) of helix B. Since FIS is involved in the regulation of many genes, its intracellular pool, which is regulated by its expression and degradation rates, may be altered by a change in FIS stability and/or a more flexible DNA binding region. Our observation of a drastic increase in the proteolytic susceptibility of the C-terminus of P61A suggests that this region may be susceptible to similar degradation events in vivo with potentially adverse functional effects.

Evidence for the three-state denaturation mechanism of P61A FIS is less direct due to the lack of a biphasic transition or of clearly nonsuperimposable transitions when monitored by different spectroscopic probes. Nevertheless, our observation of a concentration-dependent decrease in *m* value, coupled with global analysis of the data, clearly favors a three-state denaturation mechanism involving a dimeric intermediate for P61A FIS. The alteration of a protein's equilibrium denaturation mechanism by a single mutation, as shown here for P61A FIS, is quite rare and has only been seen in a few cases (*60*, *61*). The 3D structure of FIS (Figure 1) and the intramolecular interactions of the C and D helices suggest that the structure of the P61A FIS dimeric intermediate is likely to comprise helices A and B, which make up the FIS dimer core. It is noteworthy that had we carried out our experiments at only two different protein concentrations, as is commonly done in similar studies to show concentration dependence, we would not have been able to identify this subtle change in denaturation mechanism. Therefore, these results emphasize the importance of studying the equilibrium denaturation of oligomeric proteins over a wide concentration range, as well as highlighting the usefulness of global fitting for analyzing complex denaturation data. Finally, our data modeling (Figure 8) predicts that the denaturation transition of P61A FIS is expected to vary from two-state like at low protein concentration to biphasic at very high protein concentration. Since the concentrations at which P61A FIS would exhibit a biphasic transition are not experimentally feasible, it would be interesting to make destabilizing mutations at the C-terminus of P61A FIS in an attempt to fully decouple its denaturation from that of the A/B helices and observe a biphasic transition at viable FIS concentrations.

ACKNOWLEDGMENT

Our thanks to Osman Bilsel for help and advice with the program SAVUKA, to Julie Stenken for critical reading of the manuscript, to Dmitri Zagorevski for mass spectrometry analyses, and to the Department of Chemistry for support of the mass spectrometry facility. The MALDI-TOF mass spectrometer was purchased through an NSF grant (CHE-0078056).

REFERENCES

1. Yun, R. H., Anderson, A., and Hermans, J. (1991) *Proteins 10*, 219−228.
2. Hurley, J. H., Mason, D. A., and Matthews, B. W. (1992) *Biopolymers 32*, 1443−1446.
3. Kim, M. K., and Kang, Y. K. (1999) *Protein Sci. 8*, 1492−1499.
4. Chou, P. Y., and Fasman, G. D. (1978) *Adv. Enzymol. Relat. Areas Mol. Biol. 47*, 45−148.
5. Barlow, D. J., and Thornton, J. M. (1988) *J. Mol. Biol. 201*, 601−619.
6. Yuan, H. S., Wang, S. S., Yang, W.-Z., Finkel, S. E., and Johnson, R. C. (1994) *J. Biol. Chem. 269*, 28947−28954.
7. de Lamotte-Guery, F., Pruvost, C., Minard, P., Delsuc, M. A., Miginiac-Maslow, M., Schmitter, J. M., Stein, M., and Decottignies, P. (1997) *Protein Eng. 10*, 1425−1432.
8. Hardy, J. A., and Nelson, H. C. (2000) *Protein Sci. 9*, 2128−2141.
9. Brandl, C. J., and Deber, C. M. (1986) *Proc. Natl. Acad. Sci. U.S.A. 83*, 917−921.
10. von Heijne, G. (1991) *J. Mol. Biol. 218*, 499−503.
11. Sansom, M. S., and Weinstein, H. (2000) *Trends Pharmacol. Sci. 21*, 445−451.
12. Tieleman, D. P., Shrivastava, I. H., Ulmschneider, M. R., and Sansom, M. S. (2001) *Proteins 44*, 63−72.
13. Alber, T., Bell, J. A., Sun, D. P., Nicholson, H., Wozniak, J. A., Cook, S., and Matthews, B. W. (1988) *Science 239*, 631−635.
14. Finkel, S. E., and Johnson, R. C. (1992) *Mol. Microbiol. 6*, 3257−3265.
15. Osuna, R., Lienau, D., Hughes, K. T., and Johnson, R. C. (1995) *J. Bacteriol. 177*, 2021−2032.
16. Beach, M. B., and Osuna, R. (1998) *J. Bacteriol. 180*, 5932−5946.
17. Johnson, R. C., Bruist, M. F., and Simon, M. I. (1986) *Cell 46*, 531−539.
18. Koch, C., and Kahmann, R. (1986) *J. Biol. Chem. 261*, 15673−15678.
19. Haffter, P., and Bickle, T. A. (1987) *J. Mol. Biol. 198*, 579−587.
20. Thompson, J. F., Moitoso de Vargas, L., Koch, C., Kahmann, R., and Landy, A. (1987) *Cell 50*, 901−908.
21. Ball, C. A., and Johnson, R. C. (1991) *J. Bacteriol. 173*, 4027−4031.
22. Dorgai, L., Oberto, J., and Weisberg, R. A. (1993) *J. Bacteriol. 175*, 693−700.
23. Ball, C. A., Osuna, R., Ferguson, K. C., and Johnson, R. C. (1992) *J. Bacteriol. 174*, 8043−8056.
24. Xu, J., and Johnson, R. C. (1995) *J. Bacteriol. 177*, 5222−5231.

25. Ross, W., Thompson, J. F., Newlands, J. T., and Gourse, R. L. (1990) *EMBO J. 9*, 3733−3742.
26. Nilsson, L., Vanet, A., Vijgenboom, E., and Bosch, L. (1990) *EMBO J. 9*, 727−734.
27. Muskhelishvili, G., Buckle, M., Heumann, H., Kahmann, R., and Travers, A. A. (1997) *EMBO J. 16*, 3655−3665.
28. Yuan, H. S., Finkel, S. E., Feng, J. A., Kaczor-Grzeskowiak, M., Johnson, R. C., and Dickerson, R. E. (1991) *Proc. Natl. Acad. Sci. U.S.A. 88*, 9558−9562.
29. Kostrewa, D., Granzin, J., Koch, C., Choe, H. W., Raghunathan, S., Wolf, W., Labahn, J., Kahmann, R., and Saenger, W. (1991) *Nature 349*, 178−180.
30. Safo, M. K., Yang, W. Z., Corselli, L., Cramton, S. E., Yuan, H. S., and Johnson, R. C. (1997) *EMBO J. 16*, 6860−6873.
31. Osuna, R., Finkel, S. E., and Johnson, R. C. (1991) *EMBO J. 10*, 1593−1603.
32. Koch, C., Ninnemann, O., Fuss, H., and Kahmann, R. (1991) *Nucleic Acids Res. 19*, 5915−5922.
33. Ri, Y., Ballesteros, J. A., Abrams, C. K., Oh, S., Verselis, V. K., Weinstein, H., and Bargiello, T. A. (1999) *Biophys. J. 76*, 2887−2898.
34. Dmitriev, O. Y., and Fillingame, R. H. (2001) *J. Biol. Chem. 276*, 27449−27454.
35. Beach, M. (2000) in *Biology*, University at Albany, SUNY, Albany.
36. Barik, S., and Galinski, M. S. (1991) *BioTechniques 10*, 489−490.
37. Sambrook, J., Fritsch, E. F., and Maniatis, T. (1989) *Molecular Cloning: a laboratory manual*, 2nd ed., Cold Spring Harbor Laboratory, Cold Spring Harbor, NY.
38. Hobart, S. A., Ilin, S., Moriarty, D. F., Osuna, R., and Colon, W. (2002) *Protein Sci. 11*, 1671−1680.
39. Pace, C. N., Vajdos, F., Fee, L., Grimsley, G., and Theronica, G. (1995) *Protein Sci. 4*, 2411−2423.
40. Pace, C. N., Shirley, B. A., and Thomson, J. A. (1990) in *Protein Structure: A Practical Approach* (Creighton, T. E., Ed.) pp 311−330, Oxford University Press, Oxford.
41. Eftink, M. R. (1994) *Biophys. J. 66*, 482−501.
42. Bothner, B., Dong, X. F., Bibbs, L., Johnson, J. E., and Siuzdak, G. (1998) *J. Biol. Chem. 273*, 673−676.
43. Schellman, J. A. (1978) *Biopolymers 17*, 1305−1322.
44. Schellman, J. A. (1987) *Annu. Rev. Biophys. Biophys. Chem. 16*, 115−137.
45. Bilsel, O., Zitzewitz, J. A., Bowers, K. E., and Matthews, C. R. (1999) *Biochemistry 38*, 1018−1029.
46. Zitzewitz, J. A., Bilsel, O., Luo, J., Jones, B. E., and Mattews, C. R. (1995) *Biochemistry 34*, 12812−12819.
47. Bevington, P. R. (1969) *Data reduction and error analysis for the physical sciences*, McGraw-Hill Book Co., New York.
48. Gualfetti, P. J., Bilsel, O., and Matthews, C. R. (1999) *Protein Sci. 8*, 1623−1635.
49. Mulkerrin, M. G. (1996) in *Spectroscopic Methods for Determining Protein Structrue in Solution* (Havel, H. A., Ed.) pp 5−15, VCH Publishers, New York.
50. Dolgikh, D. A., Gilmanshin, R. I., Brazhnikov, E. V., Bychkova, V. E., Semisotnov, G. V., Venyaminov, S. Y., and Ptitsyn, O. B. (1981) *FEBS Lett. 136*, 311−315.
51. Harris, D. C. (1998) in *Quantitative Chemical Analysis*, pp 69−81, W. H. Freeman and Co., New York.
52. Carra, J. H., Anderson, E. A., and Privalov, P. L. (1994) *Biochemistry 33*, 10842−10850.
53. Godbole, S., Dong, A., Garbin, K., and Bowler, B. E. (1997) *Biochemistry 36*, 119−126.
54. Soulages, J. L. (1998) *Biophys. J. 75*, 484−492.
55. Spudich, G., and Marqusee, S. (2000) *Biochemistry 39*, 11677−11683.
56. Park, Y. C., and Bedouelle, H. (1998) *J. Biol. Chem. 273*, 18052−18059.
57. Stroppolo, M. E., Malvezzi-Campeggi, F., Mei, G., Rosato, N., and Desideri, A. (2000) *Arch. Biochem. Biophys. 377*, 215−218.
58. Ohgushi, M., and Wada, A. (1983) *FEBS Lett. 164*, 21−24.
59. Fontana, A., Zambonin, M., Polverino de Laureto, P., De Filippis, V., Clementi, A., and Scaramella, E. (1997) *J. Mol. Biol. 266*, 223−230.
60. Mann, C. J., Royer, C. A., and Matthews, C. R. (1993) *Protein Sci. 2*, 1853−1861.
61. Zhu, H., Celinski, S. A., Scholtz, J. M., and Hu, J. C. (2001) *Protein Sci. 10*, 24−33.
62. Kraulis, P. J. (1991) *J. Appl. Crystallogr. 24*, 946−950.

BI0265224